Proceedings of the 17th World Congress
The International Federation of Automatic Control
Seoul, Korea, July 6-11, 2008

External Force Assisted Nanorobotic Assembly of 3-D Helical Nanobelts

Gilgueng Hwang*,, Lorenzo Bagutti*, Hideki Hashmoto****

*Institute of Robotics and Intelligent Systems, ETH Zurich, 8092 Zurich , Switzerland,
(e-mail: hwangg@ethz.ch)
** Institute of Industrial Science, The University of Tokyo, 4-6-1 Komaba, Meguro-ku, Tokyo, Japan,
(e-mail: hwangkk@hlab.iis.u-tokyo.ac.jp)

Abstract: In this paper three-dimensional (3-D) suspended helical nanobelts (HNBs) with ultra-high flexibility are assembled by the external field guidance. Electromagnetic (EM) and electrostatic (ES) force by external potential are characterized quantitatively to guide the assembly of HNBs to create force sensing probe. Both ends of HNBs and target electrodes are attached with ferromagnetic metal connector. By the help of this hybrid nanorobotic assembly approach, we could successfully create force sensing probe by aligning and closing HNBs in vertical way and soldering to interconnect HNBs onto electrodes. Adhesive force between HNBs and electrodes are characterized to show its assembly performance quantitatively. The demonstrated approach shows that external force assisted assembly is an effective way for assisting serial nanorobotic assembly, interconnection soldering which may potentially reduce the production cost and time for future manufacturing realization.

1. INTRODUCTION

Three dimensional (3-D) helical structures with micro- and nano-features have been synthesized from different materials recently. The most extensively investigated ones include microcoils from amorphous carbon (Motojima et al.,1990), helical carbon nanotubes (Zhang et al.,1994), zinc oxide nanobelts (Gao et al.,2005, Kong et al.,2003), and rolled-up semiconductor helixes (Bell et al.,2006a,b). Helical structures have desirable properties which can be useful to be the building blocks of nano electromechanical systems (NEMS) sensors, actuators, springs, elecromagnets, inductors, resonators, etc.

However, 3-D helical structures prevent batch processing based on conventional 2-D microelectromechanical systems (MEMS) fabrication technology. Therefore, assembly technologies of 3-D helical structures must be developed for building MEMS/NEMS devices. To answer this question self-assembly could be one direction. In the literature self-assembly of one-dimensional (1D) nanostructures such as nanowires (NWs) and nanotubes (NTs) have been shown but with less success rate (Huang et al.,2001,Tanase et al.,2002,Niyogi et al.,2004,Agarwal et al.,2005). Major applications can be found in nanoelectronics and photonics. While it has much higher yield for generating regular patterns, it is not complex system oriented. Furthermore, self-assembly system configuration modification takes time and also very expensive, which is not feasible to quickly changing modern industry. These approaches are not mature enough to assemble 3D helical nanostructures.

However interconnection soldering problem should first be solved to create the prototype NEMS devices based on this technology. Since conventional hybrid nanorobotic approaches still remains much stressful manipulation process

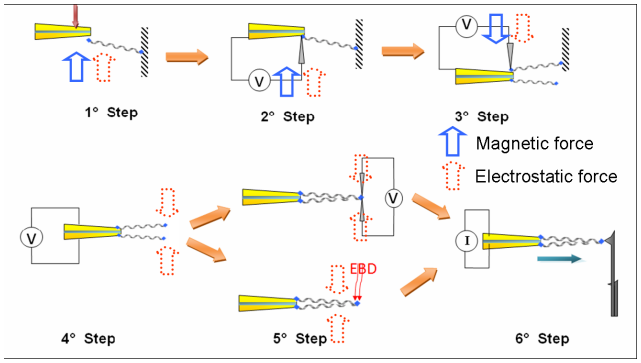

Fig. 1. Nanorobotic assembly schematic illustration of force sensing probe schematic (blue solid arrow: EM force, red dotted arrow: ES force), Step 1(attaching one side), step 2(soldering), step 3(attaching and soldering), step 4(ES pull-in), step 5(soldering by electron beam deposition), and step 6(characterization)

by human operator, results are different by user`s proficiency for especially in contact manipulation such as soldering and etc. Recently interconnection problem and soldering (spot welding, nanoink soldering and etc.) of individual nano structures with various stiffness have been studied (Dong et al.,2007, Hwang et al.,2007). Especially helical nanobelts` (HNBs) flexible structures are well known that it can easily change the shape by an external field (Shin et al.,2006) which makes these contact type soldering technologies difficult. Therefore, it is strongly required to support assistance to user`s nanorobotic manipulation while these operations. In this paper we report the mechanical characterization and assembly of HNBs by external electromagnetic (EM) force and electrostatic (ES) force for assembly. Fig. 1 shows the proposed method. It is promising to assist the interconnection soldering of flexible nanostructures such as HNBs.

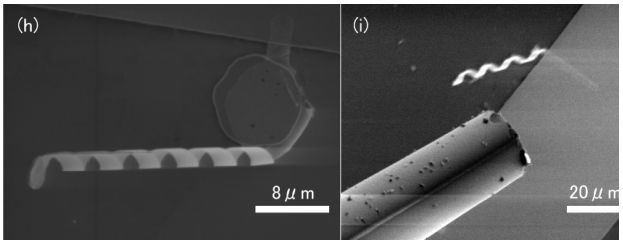

Fig. 2. As fabricated (a) InGaAs/GaAs HNBs with ferromagnetic metal pads and (b) ferromagnetic electrodes onto micro tapered pipette

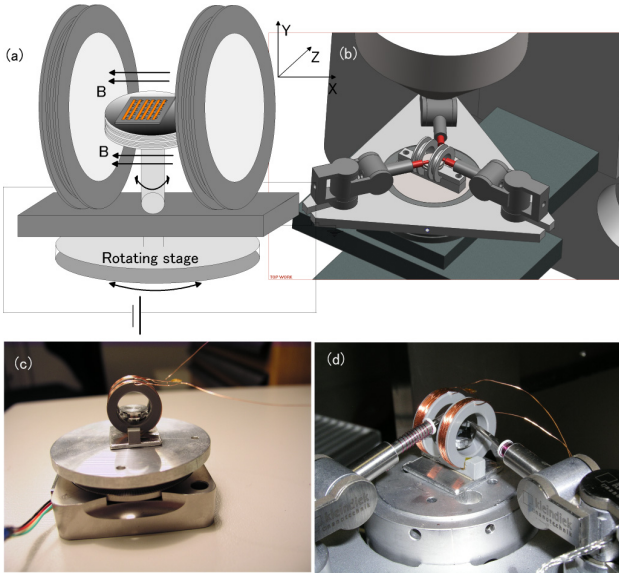

Fig. 3. Experimental setup: (a) Helmholtz coil on piezoelectric rotational stage, (b) CAD model of integration with manipulators, (c)(d) Manipulators and Helmholtz coil installed inside SEM

2. FIELD ASSISTED NANOMANIPULATION

2.1 Assembly Parts Fabrications

NEMS using HNBs include two typical configurations (Dong et al.,2006a), i.e., a HNB bridging horizontally between two electrodes or "standing" vertically onto electrodes. An as-fabricated HNB is shown in Fig. 2(a). To have a better interconnection conductivity, HNBs were fabricated with metal connectors (Cr/Ni/Au 20/200/25nm) on both ends, which is different from the "standard" design from the previous work (Bell et al.,2007). Micro tapered pipette type of electrodes have been prepared (Kim et al.,1999). Ferromagnetic Ni layer was evaporated at the end of HNB for EM actuation. Fig. 2(b) shows the as-fabricated pipette electrodes to assemble HNBs. The electrode pattern was generated by thin film evaporation. As we are aiming at assembling suspended HNBs to the as-fabricated pipette electrodes (Fig. 2(b)), Cr/Ni/Au deposited independent electrodes for precise locating of HNBs with metal deposited connectors. Firstly, the borosilicate capillary was pulled to make tapered micropipettes. The dimensions of the pipette opening can be controlled in a reproducible way by using a micropipette puller (DMZ Universal Puller, Zeitz Instruments, Germany). Pipettes with 1 and 15 μ m opening were fabricated. Then, independent Cr/Ni/Au metal layers are evaporated on both sides of pipette by changing an exposure to the target electron beam heated metal source. A home-made pipette holder with wiring is used to move using nanomanipulator and connect to the power supply.

2.2 External Force Generating System

The nanorobotic manipulation system shown in Fig. 3 has been used for the manipulation of the as-fabricated HNBs inside a scanning electron microscope (SEM) (Carl Zeiss DSM 962). Three nanorobotic manipulators (Kleindiek, MM3A) are installed inside the SEM; each has three degrees of freedom, and 5 nm, 3.5 nm, and 0.25 nm resolution in X, Y, and Z directions at the tip. A metal probe (Picoprobe, T-4-10-1 mm, tip radius: ~100nm) mounted on the nanomanipulator.

We designed a Helmholtz coil to generate required external magnetic force to assemble the HNB (Fig. 3). To be used inside the SEM chamber, we should consider the working distance of electron-beam and sample stage. 21mm diameter of ring are used to wind coils and this coil should be grounded onto sample stage to prevent charging from electron beam. Single SEM sample holder is located between two coils. Samples are placed onto the sample holder between two coils. With this coil configuration, we measured 2mT magnetic field at 2.3V, 0.254A which is required to deflect the magnetic pads on both ends of HNB. Sample holder is also coiled to have vertical axis magnetic field which obtains 1.3mT at 2V, 0.554A. This coil is mounted onto the piezo-actuated rotating nanostage as shown in Fig. 3. Two nanomanipulators are installed through the coils to work over the sample chip. We have experienced SEM imaging distortion over 5.5V which cause the heating and evaporates the parts.

2.3 Field Assisted Assembly Process of HNBs

We demonstrate the assembly of prototype force sensing probe using HNBs. A schematic of whole assembly procedure is shown in Fig. 1. The external ES and EM forces are assisting the trapping of HNB onto the electrode, soldering steps and finally the closing the aligned HNBs. Once independent metal layers for electrodes are fabricated onto the pipette, nanoink is pre-deposited onto the both ends of pipette tip. Then, it is installed into the nanorobotic manipulators using a custom connector for electrical circuiting. A pipette attached to the manipulator is made to contact with the suspended HNB metal pad on the chip. In-situ nanoink soldering with fresh 2nd probe tip was then performed. A single HNB is assembled onto an electrode with ohmic contact and released by breaking the attached side by the probe (Fig. 1 1st and 2nd step). Both of ES and EM force are applied during the contact soldering. The 3rd step shows the other side of HNB assembly using the same

method with a 3rd probe tip. The released both ends of attached two HNBs are assembled by applying ES pull-in voltage (37 V) (Fig. 1 4th step). The proper pull-in voltage can be calculated in simulation using the geometry model of HNBs and pipette tip opening. The closed two metal pads of HNBs are deposited with electron beam deposition (EBD) (Fig. 1 5th step). Both of EM and ES field are assisting nanorobotic manipulation using proposal system.

3. CHARACTERIZATIONS

3.1 Mechanical Stability Characterization

We first estimated an EM attracting force between probe tip and HNB Ni pad. A probe is approached to the HNB pad without applying EM field and then generate field to have an EM attracting force. Once HNB gets to be closed, this force can be estimated from the HNB deflection measurement when we measured till it loses its bond. We used HNB with 6 turns which has stiffness referenced from the previous characterization (Bell et al.,2006b). Then, by the measured HNB`s maximum deflection, we can estimate the maximum interaction force by the external EM field analytically.

$$B = \left(\frac{4}{5}\right)^{\frac{3}{2}} \frac{\mu_0 nI}{R} \qquad (1)$$

Eq. 1 describes the magnetic flux density B from the Helmholtz coil configuration. We can analyze the B and its distribution over voltage from 0 to 3V to know the maximum

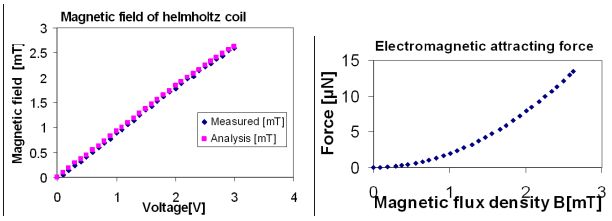

(a) (b)

Fig. 4. Electromechanical characterization of magnetic nanospring: (a) Magnetic field measurement of Helmholtz coil, (b)Magnetic attracting force between probe and Ni pad

range. Fig. 4(a) shows the analytical field estimation and measured field by gauss meter (GM05, Hirst magnetic instrument. LTD). It is linear and closely related between analytic and measured data. We used Eq. 2 to estimate the force between two very close attracting surfaces which is probe tip and magnetic pads attached to both ends of HNB. We assume that full area of Ni pad is attached to probe to simplify the contact model. Fig. 4(b) depicts the EM attracting force distribution between probe and Ni pad of HNB`s both ends. Analytical results show that we can have a 15μN attracting force between two metal contacts by less than 3mT field.

$$F = \frac{AB^2}{2\mu_0} \qquad (2)$$

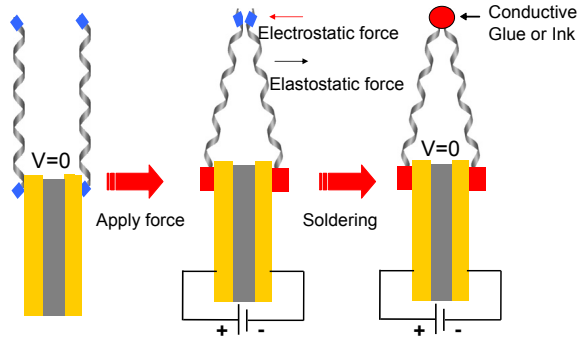

Fig. 5. HNB assembly force diagram: Force balance for HNBs over a electrode: (a) position of the HNB when V = 0 (left), (b) deformed position of the HNB when $V \neq 0$ (middle), and (c) assembled HNB by soldering

where,

B is magnetic flux density between two coils in tesla [T]

μ_0 is the permeability of space, which equals $4\pi \times 10^{-7}$ tesla · meter/ampere

n is the number of turns in each coil

I is the current flowing through the coil in ampere [A]

A is the contact area of each surface, in m^2

We used the Helmholtz coil with 100 turns and area of surface contact of HNB pad is obtained with the 2.5μm diameter circular pad. Then, we made an experiment of measuring this attracting force between probe tip and metal pads of HNB. We first approach the probe using piezo actuated nanomanipulator to the HNB suspended inside the SEM vacuum chamber. We minimized other interacting force such as ES force by grounding the manipulator feed through and trying to make a several approach to ground it and contact to the substrate which is conductive to the sample stage by discharging it. We still experience very weak interaction force between pads and probe from van der waals force and electron beam charging even without applying magnetic field. However, it is not enough to make the HNB mechanically deflect itself without very closely located charged objects, so we can ignore it since we measure the interacting force by the maximum elongation when it is in contact mode under an external magnetic field. We first elongate the nanobelt attached probe. Maximum elongation under different strength of an EM field is measured. For example, maximum elongation before we lose contact is measured as 41μm which is 64% elongated from the initial length 25μm. At this time, we applied 2.6V, 0.285A to generate 2.291mT over the coil which is curve fitted from the previously obtained force estimation (Bell et al.,2006b). This 64% maximum elongation corresponds to the curve fitted result which is around 11~12 μN. The stiffness and force of HNB change by nonlinear relation to the given elongation. We compared with the force estimation result of InGaAs/GaAs bilayer HNB that we used in the experiment too. This force (11~12μN) is high enough to break the

attracting force (10.7μN) under this field (Fig. 4(b)). EM attracting force is estimated close to the analytical model.

3.2 Field Assisted Assembly characterization

Fig. 5 shows the physical operation of a HNB-based force sensing probe assembly. When a potential difference is created between both the HNBs assembled onto electrode, ES charges give rise to ES force which deflects the HNBs. In addition to ES force, van der Waals force can also affect to the HNB deflection depending on the gap between vertically aligned HNBs. Elastic force which can restore the HNB to its original straight position counteracts against both the ES and van der Waals. For an applied voltage, an equilibrium position is given by the balance of the elastic, ES and the van der Waals force. When the applied potential difference between two HNBs exceeds a certain potential, the HNBs become unstable and collapses each other. The potential at this time is defined as the pull-in voltage or the collapse voltage.

ES force: HNBs are approximated as a perfect cylinder with HNB`s Young`s modulus for the calculation simplicity. The capacitance per unit length for the cylindrical beam over the HNBs is given by (Ke et al.,2005 and Dequesnes et al.,2002):

$$C(r) = \frac{\pi\varepsilon_0}{\log\left[1 + \frac{r}{R} + \sqrt{(\frac{r}{R}+1)^2 - 1}\right]} \qquad (3)$$

where R is the radius of the cylinder/conductor, r is the gap between both HNBs and ε_0 is the permittivity of vacuum. The ES energy per unit length is given by $E_{elec}/L = CV^2/2$. The ES force per unit length, q_{elec} is then given by:

$$q_{elec} = \frac{\pi\varepsilon_0 V^2}{R\sqrt{\frac{r(r+2R)}{R^2}}\log^2\left[1 + \frac{r}{R} + \sqrt{\frac{r(r+2R)}{R^2}}\right]} \qquad (4)$$

Elastostatic domain: The mechanical behaviour of the HNB is approximated by a continuum beam equation, i.e.

$$EI\frac{d^4r}{dx^4} = q \qquad (5)$$

where r is the gap between two HNBs, x is the position along the HNB, q is the force per unit length acting normal to the beam, E is the Young`s modulus, I is the moment of inertia and for HNB can be estimated as

$$I = \pi/4 \times (R_{ext}^4 - R_{\text{int}}^4) \qquad (6)$$

where R_{int} is the interior radius and R_{ext} is the exterior radius. In the eq. 5 we put instead of q the eq. 6 and then we solve that to find the deflection r(x,V) in function of the distance and the voltage.

4. EXPERIMENTS

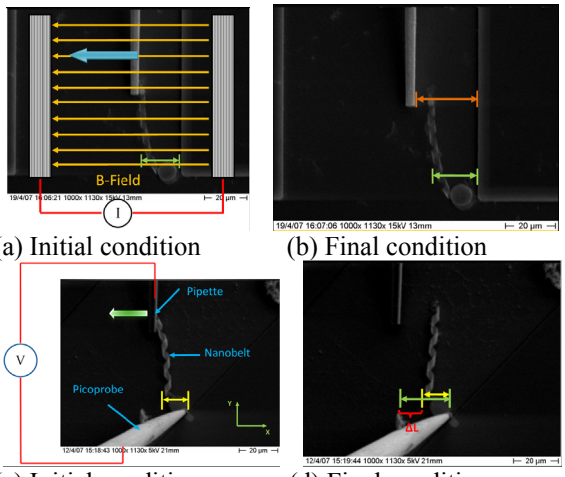

(a) Initial condition (b) Final condition

(c) Initial condition (d) Final condition

Fig. 6. Experiment: the deflection of the HNB by EM force (a,b), the deflection of the HNB by ES force (c,d)

4.1 Deflection experiment with ES force

Finite element method (FEM) simulation was used to estimate the applied force onto HNBs for experiments. The dimensions of the HNBs used in the simulation were the same as in the experiments, as summarized in Table I. The simulation result has previously been validated with experimental results for similar structures (Bell et al., 2006b). Simulation was carried out in the linear elastic range (small displacements). Values of the materials properties in the model were taken from Ref. (Bell et al.,2006b and Nakajima, 1999) with the rule of mixture applied for the InGaAs layer. Both ends of the helix were constrained from rotation around all three axes. Moreover, on one end it was constrained from all translational movements, and on the other end it was constrained from translational movement perpendicular to the axis. On this end, a force in the axial (X-axis) or bending (Y-axis) direction was applied to compute the displacement. In Fig. 7, a plot of the displacement along the bending direction is shown. From the simulation, bending stiffness of the structure is determined to be 0.0001 N/m as summarized in Table I.

Table I. Specifications of HNBs used for simulation

Length [μm]	36.3
Radius [μm]	1.05
Pitch [μm]	6.6
Width [μm]	3
# of turns	5.5
Stiffness [N/m]	0.0001
Force [pN]	0.001 – 1

The first thing to do is the preparation of the sample and the installation of the manipulators. In fact, if the pipette is touched barehanded, without protections, it can happen that the electrostatic discharge (ESD) breaks the thin part of the pipette. For this reason, a bracelet and special gloves were used to ground it during the installation. In Fig. 6 we can see that the probe is in contact and made in electric circuit with the suspended HNB. The HNB plays the role of switch. In Fig. 6(c) the circuit is closed in the second Fig. 6(d) is open.

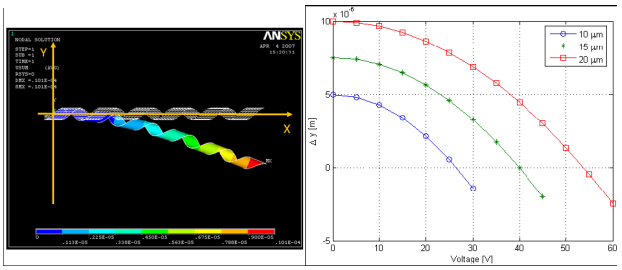

Fig. 7. FEM simulation of HNB by ANSYS: (a) bending force simulation for HNBs closing. (b) voltage in function of the HNB's deflection for different gaps (10µm, 15µm, 20µm)

The pipette has to be as near as possible until it touches the HNB (the circuit is closed). At this point an SEM image was grabbed for initial state. Then the pipette is moved away from the present position on y-axis until the contact between the pipette and the HNB is broken and another new image was grabbed. In the end two images (Fig. 6) are compared to find how much the HNB was deflected (Δ d). This procedure was repeated with different voltages. When all the results were analyzed (Voltage or current versus Δ d), we finally obtain the curve shown in Fig. 8(a). It shows linear relation between

Table II Experiments specifications

Gap r [μ m]	5
Length [μ m]	36.3
R_{ext} [μ m]	1.05
R_{int} [μ m]	1.023
Electric Constant e_0 [C^2/Nm^2]	$8.85 \cdot 10^{-12}$
Voltage Range V [V]	0-1; Step: 0.1 V
E-Modul [N/m^2]	$8.0215 \cdot 10^{10}$

the voltage and the deflection except a drop at 8V which was caused by an unequal contact configuration.

4.2 Deflection experiment with EM force

The next experiment that will be mentioned, it is similar to the previous tests (Section 4.1). This time however we use helmholtz coils to generate a uniform EM field Fig. 6. Between the coils, the sample with HNBs is mounted. The experiment consists of moving the pipette until it is in contact to the HNB. This will be the initial state, then the pipette is moved away from this position until the pipette-HNB contact is released. As was described in the previous experiment (Section 4.1), images at each time are grabbed for the deflection measurement. Deflection versus the current flowing through the Helmholtz coil gives the plot (Fig. 8(b)). It should be noted that there is a limitation of the current, as the higher current than the limit results in SEM images distortion. In fact, the curve of the plot linearly increases. It is more improved by an ESD during several try. There are still a few problems to decouple the EM force itself from ES or van der Waals force. However current result is good enough to show that EM field is contributing the magnetization of metal pad of HNBs.

Given the coil setup, we measured 2mT magnetic field at 2.3V, 0.254A. Then the resistance can be calculated using ohm`s law by R = 2.3[V] / 0.254 [A] = 9.055 [Ω]. In Fig.

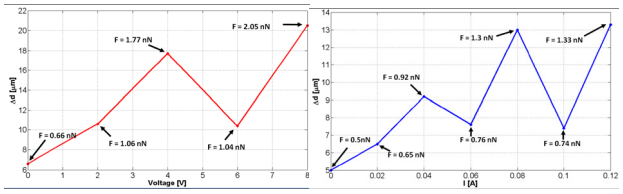

(a) ES force assistance (b) EM force assistance

Fig. 8. Experiments with ES force and EM force assistance: deflection Δd [µm]

8(b) we use the current I = 0.12 [A] to measure the Voltage: V = R· I = 1.086 [V].

For a voltage of 1.086 [V] we obtain a B-field of 0.9 [mT] from Fig 4(a). We obtain an attracting force between probe and Ni pad as 0.2 [µN] from the magnetic field of 0.9 [mT]. Then we can compare the estimated force with the experimental result in Fig. 8(b). It reads 1.33 [nN] force when the current is I = 0.12 [A]. This much big difference can be explained by the fact that the analytical result is an ideal case with surface to surface contact between metal pad and pipette. However as shown in Fig. 6, we could only make a contact in side of pad which reduce the adhesive force. We must also consider that the HNB by one side is fixed; this means that the torsion force plays a bigger role.

4.3 Force assisted closing of HNBs

In the theory we have explained the equation of the ES force (Eq.4), with it we have done a few simulations to understand the behavior of the voltage on function of the deflection. MATLAB script to calculate the force with different HNBs was prepared and it is useful for the iterative simulations. We used different gaps between HNBs, the idea of the process is likely as the one in Fig. 7. The gap distances are set as 10µm, 15µm and 20µm respectively. It should be noted that the pull-in voltage or the necessary voltage to collapse was found in the middle of the gap. It means that two HNBs are attached together at this position. In the Eq.4, we must insert the gap (r), the voltage (V) and the radius of HNB turn (R_{ext})(Table II). The calculated force using MATLAB script is utilized in the other MATLAB script to create a HNB model for the simulation in ANSYS. We must change step-by-step the force data in the file, compile and start in ANSYS the simulation per determined deflection. Finally we could have the relation between the voltage and the deflection of the HNBs. The results of this simulation are shown in these plots Fig. 7(b). The pull-in voltage of 27 V was obtained in case of 10µm gap. We should not consider the result with a negative value in the graph, because the two HNBs, when the distance 0µm is reached, are attached together so the HNB isn't able to go over this distance. We have these negative data by the ANSYS simulation because we have used a range of the voltage (for the force) without consider the limit. In the second case (15µm gap) the voltage is 40 V and the third (20µm gap) is 54V.

Whole assembly procedure inside SEM by the assistance of external field was shown in Fig. 9. A piezoresistive HNB force sensing probe was assembled using the proposed method. It was conducted by serial nanorobotic assembly

with the external electrostatic and electromagnetic force assist. The force sensing probe shows piezoresistivity by the deflection and calibrated with as-calibrated atomic force microscope cantilever.

5. CONCLUSIONS

Helical nanobelt force sensing probe was assembled using external force assisted nanorobotic assembly. Both the ES and EM force are characterized quantitatively to show its contribution to a whole assembly process. ES force is relatively stronger force than EM force in the SEM environment constraint. However the hybrid approach of using both fields can be useful for the variety of future assembly tasks requires certain amount of assembly force such as soldering and etc. The work is expected to be applied to the real assembly tasks and steps toward future autonomous nanorobotic manufacturing.

REFERENCES

Motojima, S., M. Kawaguchi, K. Nozaki, and H. Iwanaga, (1990). Growth of regularly coiled filaments by Ni catalyzed pyrolysis of acetylene, and their morphology and extension characteristics. *Applied Physics Letters*, vol. 56, pp. 321-323

Zhang, X. B., X. F. Zhang, D. Bernaerts, G. T. Vantendeloo, S. Amelincks, J. Vanlanduyt, V. Ivanov, J. B. Nagy, P. Lambin, and A. A. Lucas, (1994). The texture of catalytically grown coil-shaped carbon nanotubules. *Europhysics Letters*, vol. 27, pp. 141-146

Nakajima, K. (1999). Equilibrium phase diagrams for Stranski-Krastanov structure mode of III-V ternary quantum dots. Japanese Journal of Applied Physics Part 1 38: 1875-1883.

Gao, P. M., Y. Ding, W. J. Mai, W. L. Hughes, C. S. Lao, and Z. L. Wang, (2005). Conversion of zinc oxide nanobelts into superlattice-structured nanohelices. *Science*, vol. 309, pp. 1700-1704

Kong, X. Y., and Z. L. Wang, (2003). Spontaneous polarization-induced nanohelixes, helical nanobelts, and nanosprings of piezoelectric nanobelts. Nano Letters, vol. 3, pp. 1625-1631

Bell, D. J., Y. Sun, L. Zhang, L. X. Dong, B. J. Nelson, and D. Grützmacher, (2006). Three-dimensional nanosprings for electromechanical sensors. Sensors and Actuators A-Physical, vol. 130-131, pp. 54-61

Bell, D. J., L. X. Dong, L. Zhang, M. Golling, B. J. Nelson, and D. Grützmacher, (2006). Fabrication and characterization of three-dimensional InGaAs/GaAs nanosprings. Nano Letters, vol. 6, no. 4,pp. 725-729, 2006

Bell, D. J., Y. Sun, L. Zhang, L. X. Dong, B. J. Nelson, D. Grützmacher, (2006) Three-dimensional nanosprings for electromechanical sensors, Sensors and Actuators A, vol. 130, pp. 54-61

Bell, D. J., T. E. Bauert, L. Zhang, L. X. Dong, Y. Sun, B. J. Nelson, and D. Grützmacher, (2007) Directed batch assembly of three-dimensional helical nanobelts through angular winding and electroplating, Nanotechnology, vol. 18, no. 5, art. no. 055304

Hwang, G., C. Dockendorf, D. Bell, L. Dong, H. Hashimoto, D. Poulikakos and B. Nelson, (2007). In-situ Nanorobotic Soldering of Three-dimensional Helical Nanobelts using Gold Nanoink. Prof. of IEEE Intl. Conf. on Nanotechnology, pp. 813-818.

Ke. C. H., N. P., B. Peng, H. D. Espinosa (2005). Experiments and modeling of carbon nanotube-based NEMS devices. Journal of Mechanics and Physics of solids 53: 1314-1333.

Dequesnes. M., S. V. R., and N. R. Aluru (2002). Calculation of pull-in voltages for carbon-nanotube-based nanoelectromechanical switches. Nanotechnology 13: 120-131.

Shin. M., S. K., and S. Kim (2006). Controlled assembly of polymer nanofibers: From helical springs to fully extended. Applied Physics Letters 88(223109): 1-3.

Tanase. M., D. M. S., A. Hultgren, L. A. Bauer, P. C. Searson, G. J. Meyer, and D. H. Reich (2002). Magnetic trapping and self-assembly of multicomponent nanowires. Journal of Applied Physics 91(10): 8549-8551.

Kim, P., a. C. M. L. (1999). Nanotube Nanotweezers. Science 286(5447): 2148-2150.

Agarwal. R., K. L., Y. Roichman, G. Yu, C. M. Lieber, and D. G. Grier (2005). Manipulation and assembly of nanowires with holographic optical traps. Journal of Optics Express 13(22).

Huang, Y., C. M. Lieber, (2001). Directed Assembly of One-Dimensional Nanostructures into Functional Networks. Science 291: 630-633.

Niyogi. S., C. H., R. M. Thamankar, Y. Chaiang, R. Kawakami, N. V. Myung, and R. C. haddon (2004). Magnetically Assembled Multiwalled Carbon Nanotubes of Ferromagnetic Contacts. Journal of Physics Chemistery B 108: 19818-19824.

Vikramaditya, B., B. J. Nelson, G. Yang, and E. Enikov, (2001). Microassembly of Hybrid Magnetic MEMS. Journal of Micromechatronics. Vol. 1, No. 2, pp. 99 – 116

Dong, L., L. Zhang, D. J. Bell, B. J. Nelson, and D. Grutzmacher, (2006) Hybrid nanorobotic approaches for fabricating NEMS from 3D helical nanostructures, Proc. Of IEEE Intl. Conf. of Robotics and Automation, pp. 1396-1401

Dong, L., X. Y. Tao, L. Zhang, B. J. Nelson, X. B. Zhang, (2007) Nanorobotic spot welding: controlled metal deposition with attogram precision from copper-filled carbon nanotubes, Nano Letters, vol. 7, no. 1, pp. 58-63